

X-ray Limits on the Progenitor System of the Type Ia Supernova 2017ejb

Charles D. Kilpatrick^{1*}, David A. Coulter¹, Georgios Dimitriadis¹, Ryan J. Foley¹, David O. Jones¹, Yen-Chen Pan¹, Anthony L. Piro², Armin Rest^{3,4}, César Rojas-Bravo¹

¹*Department of Astronomy and Astrophysics, University of California, Santa Cruz, CA 95064, USA*

²*The Observatories of the Carnegie Institution for Science, 813 Santa Barbara St., Pasadena, CA 91101, USA*

³*Space Telescope Science Institute, 3700 San Martin Drive, Baltimore, MD 21218, USA*

⁴*Department of Physics and Astronomy, The Johns Hopkins University, 3400 North Charles Street, Baltimore, MD 21218, USA*

Accepted 0000, Received 0000, in original form 0000

ABSTRACT

We present deep X-ray limits on the presence of a pre-explosion counterpart to the low-luminosity Type Ia supernova (SN Ia) 2017ejb. SN 2017ejb was discovered in NGC 4696, a well-studied elliptical galaxy in the Centaurus cluster with 894 ks of *Chandra* imaging between 14 and 3 years before SN 2017ejb was discovered. Using post-explosion photometry and spectroscopy of SN 2017ejb, we demonstrate that SN 2017ejb is most consistent with low-luminosity SNe Ia such as SN 1986G and SN 1991bg. Analyzing the location of SN 2017ejb in pre-explosion images, we do not detect a pre-explosion X-ray source. We use these data to place upper limits on the presence of any unobscured supersoft X-ray source (SSS). SSS systems are known to consist of white dwarfs accreting from a non-degenerate companion star. We rule out any source similar to known SSS systems with $kT_{\text{eff}} > 85$ eV and $L_{\text{bol}} > 4 \times 10^{38}$ erg s⁻¹ as well as models of stably-accreting Chandrasekhar-mass WDs with accretion rates $\dot{M} > 3 \times 10^{-8} M_{\odot}$ yr⁻¹. These findings suggest that low-luminosity SNe Ia similar to SN 2017ejb explode from WDs that are low-mass, have low pre-explosion accretion rates, or accrete very soon before explosion. Based on the limits from SN 2017ejb and other nearby SNe Ia, we infer that <47% of SNe Ia explode in stably-accreting Chandrasekhar-mass SSS systems.

Key words: supernovae: general — supernovae: individual (SN 2017ejb) — X-rays: general

1 INTRODUCTION

Type Ia supernovae (SNe Ia) are a homogeneous class of SNe defined by a lack of hydrogen and helium in their spectra but with strong silicon absorption (for a review see, e.g. Filippenko 1997). For over 50 years, the leading progenitor model for SNe Ia has been a white dwarf (WD) that undergoes a thermonuclear explosion (Hoyle & Fowler 1960; Finzi & Wolf 1967; Hansen & Wheeler 1969). The pathway by which these WDs ignite is less certain. Potential models include the merger of two carbon/oxygen WDs (Iben & Tutukov 1984; Webbink 1984), accretion and detonation of a helium shell on a sub-Chandrasekhar WD (Taam 1980; Shen & Bildsten 2014), direct collision of two unbound WDs in dense stellar systems (Rosswog et al. 2009; Raskin et al. 2010; Thompson 2011; Kushnir et al. 2013), or steady accretion leading to a Chandrasekhar-mass explosion (Whelan & Iben 1973; Nomoto 1982). Even among these general classes of explosion

scenarios there are important differences, such as whether ignition in the merger case is triggered by unstable (Guillochon et al. 2010; Dan et al. 2012; Pakmor et al. 2012) or stable mass transfer (Fink et al. 2007, 2010; Shen & Bildsten 2009).

The fact that these models are all theoretically plausible and reproduce some of the observed characteristics of SNe Ia may reflect SN Ia diversity within the overall class. Despite the homogeneity of SN Ia spectroscopic features and light curve shapes, they span a range of luminosities (from low-luminosity 1991bg-like SNe Ia to high-luminosity 1991T-like and 2006gz-like SNe Ia; e.g., Phillips et al. 1999; Ashall et al. 2016), ejecta velocities (Foley & Kasen 2011; Mandel et al. 2014), abundance distributions in their outer ejecta layers (Lentz et al. 2000; Foley et al. 2016; Cartier et al. 2017), abundances inferred from nebular spectra (Mazzali et al. 2015), and large-scale environments (Cooper et al. 2009; Sullivan et al. 2010; Pan et al. 2014). Detailed predictions for how these properties depend on explosion scenario are one of the most promising avenues for determining the true explosion pathway(s) (Foley et al. 2012; Maoz et al. 2014).

* Email: cdkilpat@ucsc.edu

In addition to understanding their explosion physics, the connection between progenitor channels and SN Ia luminosity is of utmost importance for cosmology. SN Ia light curves are among the most reliable redshift-independent distance indicators out to high redshift (Jones et al. 2013; Rubin et al. 2017), and they are the basis for the discovery of the accelerating expansion of the Universe (Riess et al. 1998; Perlmutter et al. 1999). However, as we measure larger samples of SN Ia light curves with increasing precision, it has become clear that a major limiting factor in using SNe Ia to measure cosmological parameters is systematic uncertainty in how SN Ia explosion properties affect their intrinsic colors and luminosity (see analysis in Scolnic et al. 2017). A physically-motivated understanding of SN Ia evolution at all wavelengths is essential before these systematic uncertainties can be thoroughly addressed and precision in cosmological parameters is significantly improved. Fundamentally, this means isolating an explosion model and observables that break the degeneracies between SN Ia light curve shape and intrinsic luminosity.

Various explosion models predict radically different pre-explosion states for SNe Ia, including electromagnetic and gravitational signals that may be detectable from nearby systems. Inspiral-ing binary WDs produce a background of gravitational wave emission (in the 0.1–1 mHz regime) that will be targeted and potentially resolvable by *LISA* (Edlund et al. 2005). Accreting WDs with non-degenerate companion stars produce thermal emission that peaks in the ultraviolet and X-ray (Di Stefano 2010). Sufficiently massive and luminous WD companion stars may be directly observed in pre-explosion images of nearby SNe Ia (Maeda et al. 2014). These signals have been explored for some nearby systems; for example, optical pre-explosion limits (for SNe 2011fe and 2014J; Li et al. 2011; Kelly et al. 2014) have ruled out $> 5 M_{\odot}$ companions for two “normal” SNe Ia (i.e., similar to those used for cosmology in Riess et al. 2016). Many nearby galaxies are well-studied at X-ray energies with deep *Chandra* imaging, and SNe 2011fe and 2014J have deep limits on the presence of an accreting WD, also called a supersoft X-ray source (SSS), in a symbiotic binary or accreting from the wind of its companion star (Nielsen et al. 2012, 2013, 2014).

In rare cases, deep pre-explosion imaging can serendipitously lead to interesting limits on SN Ia progenitor systems, even for SNe that occur much more than 10 Mpc away (whereas, e.g., SNe 2011fe and 2014J were 7.2 and 3.5 Mpc away, respectively; Li et al. 2011; Kelly et al. 2014). This was the case for SN 2012fr, whose host galaxy was observed by *Chandra* for a total of ~ 300 ks, providing the third deepest limits on the presence of a SSS (after SNe 2011fe and 2014J) in spite of the fact that SN 2012fr is 21 Mpc away (Nielsen et al. 2013). Similarly, the host galaxy of the low-luminosity SN Iax 2012Z was observed by the *Hubble Space Telescope* (*HST*) for > 100 ks, and a blue source consistent with a non-degenerate helium companion star was identified despite the fact that it is 33 Mpc away (McCully et al. 2014). Although nearby events in well-studied galaxies typically lead to deeper limits on the presence of a progenitor system, systematic follow up of all nearby SNe Ia with pre-explosion imaging is essential to understand the progenitor population as a whole.

In this paper, we discuss SN 2017ejb, which was discovered in the elliptical galaxy NGC 4696 (the brightest galaxy in the Centaurus cluster) on 28.22 May 2017 by the $D < 40$ Mpc (DLT40) survey (Tartaglia et al. 2017)¹. Deep limits from 6 days before discov-

Table 1. *Chandra*/ACIS Data of NGC 4696

<i>Chandra</i> Observation	Epoch (start date)	Exposure (ks)	Pointing Center (α, δ) (J2000.0)
504	−6215.20	31.75	12:48:48.70, −41:18:44.00
505	−6198.22	9.96	12:48:48.70, −41:18:44.00
1560	−6248.53	84.75	12:48:49.40, −41:18:40.50
4190	−5153.68	34.27	12:49:05.00, −41:16:17.00
4191	−5153.26	34.02	12:48:41.00, −41:22:36.00
4954	−4804.64	89.05	12:48:48.90, −41:18:44.40
4955	−4803.58	44.68	12:48:48.90, −41:18:44.40
5310	−4802.04	49.33	12:48:48.90, −41:18:44.40
8179	−3716.64	29.79	12:50:03.90, −41:22:57.00
16608	−1146.49	34.11	12:48:48.90, −41:18:43.80
16224	−1144.85	42.29	12:48:48.90, −41:18:43.80
16607	−1142.20	45.67	12:48:48.90, −41:18:43.80
16625	−1127.24	30.10	12:48:48.90, −41:18:43.80
16610	−1126.34	17.34	12:48:48.90, −41:18:43.80
16609	−1119.92	82.33	12:48:48.90, −41:18:43.80
16223	−1097.25	178.97	12:48:48.90, −41:18:43.80
16534	−1087.85	55.44	12:48:48.90, −41:18:43.80

Note. Epoch is in days relative to discovery on 28.22 May 2017.

ery suggest that SN 2017ejb was first observed within a few days of explosion. Follow-up spectroscopy of SN 2017ejb on 29 May 2017 (Pan et al. 2017; Valenti et al. 2017) suggested that it was a 1991bg-like SN Ia roughly one week before maximum light.

Here, we report pre-explosion *Chandra* and *HST* imaging of the explosion site of SN 2017ejb as well as follow-up photometry and spectroscopy. Our light curves and spectra indicate that SN 2017ejb is a peculiar SN Ia with a low peak luminosity, lacks a secondary *i*-band maximum, and has strong carbon absorption at early times. Overall, this source is most similar to low-luminosity SNe Ia such as SN 1986G and SN 1991bg. We examine all pre-explosion data to look for an optical or X-ray counterpart to SN 2017ejb, but do not detect any sources. The limiting X-ray flux rules out the presence of any SSS similar to known systems with bolometric luminosity $> 4 \times 10^{38}$ erg s^{−1} or effective temperature > 85 eV. These limits rule out much of the temperature-luminosity space for SSS systems in nearby galaxies as well as models of stably-accreting Chandrasekhar-mass WDs with accretion rates $\dot{M} > 3 \times 10^{-8} M_{\odot}$ yr^{−1}.

Throughout this paper, we assume a Milky Way reddening to NGC 4696 of $E(B - V) = 0.098$ mag (Schlafly & Finkbeiner 2011) and a distance to the Centaurus cluster of $d = 41.3 \pm 2.1$ Mpc ($\mu = 33.08 \pm 0.11$ mag; Mieske & Hilker 2003).

2 OBSERVATIONS

2.1 Archival Data

2.1.1 *Chandra*

We searched for pre-explosion observations of NGC 4696 from the *Chandra* Data Archive. We found data consisting of 17 epochs of Advanced CCD Imaging Spectrometer (ACIS) images and totaling ~ 894 ks of effective exposure time. These data were obtained between 22 May 2000 and 5 Jun. 2014. We list all *Chandra* observations in Table 1.

Using the *Chandra* Interactive Analysis of Observations (CIAO) software package (Fruscione & Siemiginowska 1999), we

¹ SN 2017ejb is also called DLT17bk

merged all of these data into a single event map. We note that SSS emission is negligible above 1 keV (1.2 nm; see Di Stefano et al. 2004; Ness et al. 2013), and so following similar procedures in Nielsen et al. (2011), we limited our analysis to events in the 0.3–1.0 keV soft band of *Chandra*/ACIS. We used CIAO/merge_obs to construct event and exposure maps centered around the location of SN 2017ejb as reported in Tartaglia et al. (2017).

2.1.2 Hubble Space Telescope

The site of SN 2017ejb was also observed by the *Hubble Space Telescope* (*HST*) with the Advanced Camera for Surveys (ACS) Wide Field Channel (WFC) in *F435W* and *F814W*. These images were observed over a single epoch on 24 Aug. 2004. We obtained the individual `flc` files from the Mikulski Archive for Space Telescopes². These consisted of 4×1360 s exposures in *F435W* and 4×580 s exposures in *F814W*. Following procedures described in Kilpatrick et al. (2018), we drizzled the images together and performed photometry on the `flc` files using `dolphot` (Dolphin 2000). We used standard `dolphot` parameters for ACS³. The instrumental magnitudes were calibrated using the zero points for *HST*/ACS from 24 Aug. 2004⁴. For reference to the individual `flc` files, we drizzled all *F435W* and *F814W* together to construct the deepest image possible (*F435W*+*F814W*), which is shown in Figure 1.

2.2 Spectroscopy

We observed SN 2017ejb on 29.04 May 2017 with the Goodman Spectrograph (Clemens et al. 2004) on the 4.1 m Southern Astrophysical Research Telescope (SOAR) on Cerro Pachón, Chile. Our SOAR/Goodman setup and spectral reduction procedure are described in Kilpatrick et al. (2018). We de-reddened the spectrum for the Milky Way value and removed the recession velocity 2960 km s^{-1} , which is consistent with the redshift of NGC 4696. This spectrum is shown in Figure 2.

SN 2017ejb was also observed on 1.18 Jun 2017 with the ESO Faint Object Spectrograph and Camera (EFOSC2) on the ESO 3.6 m New Technology Telescope (NTT) at La Silla Observatory, Chile as part of the PESSTO programme⁵ (for a description of the observing programme and instrumental setup, see Smartt et al. 2015). We reduced these data following standard procedures in IRAF⁶. The final spectrum is shown in Figure 2.

We also obtained a spectrum observed with X-shooter on the Very Large Telescope (VLT) on Cerro Paranal, Chile on 9.03 June 2017⁷ (ESO programme 099.D-0641, PI Maguire). The data were processed using the latest version of the X-shooter pipeline (Modigliani et al. 2010) with calibration frames and standard star spectra obtained on the same night and in the same instrumental configuration. We combined data from the ultraviolet/blue, optical, and infrared arms of X-shooter by scaling the individual spectra

to the overlap region between each side. We show the combined spectrum in Figure 2.

2.3 Swope Imaging

We observed SN 2017ejb using the Direct CCD Camera on the Swope 1.0 m telescope at Las Campanas Observatory, Chile, between 4 Jun. 2017 and 16 Aug. 2017 in *uBVgriz*⁸. We performed standard reductions on the Swope data, including bias-subtraction, flat-fielding, cross-talk correction, astrometry, and photometry, using the `photpipe` imaging and photometry package (Rest et al. 2005) as discussed in Kilpatrick et al. (2018). We did not subtract a template from images with the SN, but we accounted for the sky and host galaxy background level by fitting to the median background level around the PSF aperture.

We calibrated the *ugri* photometry using SkyMapper secondary standards (Wolf et al. 2018) in the same field as SN 2017ejb. For our *BV* photometry, we transformed the SkyMapper standard star *gr* magnitudes to *BV* using transformations in Jester et al. (2005). SN 2017ejb was clearly detected in each epoch at the coordinates reported in Tartaglia et al. (2017). The final photometry of SN 2017ejb is presented in Table 2 and shown in Figure 3.

3 PHOTOMETRIC AND SPECTRAL CLASSIFICATION OF SN 2017EJB

3.1 Spectroscopic Classification

In Figure 2, we show all of our spectral epochs of SN 2017ejb with several spectroscopic features identified. At 8 days before *B*-band maximum (as determined in Section 3.2), our SN 2017ejb spectrum exhibits prominent lines of Si II, S II, Ca II, and C II, which indicate that SN 2017ejb is a SN Ia. We only detect C II absorption in our first spectroscopic epoch, roughly 8 days before *B*-band maximum. While the presence of the C II $\lambda 6580$ feature and possible detection of C II $\lambda 7234$ in SN 2017ejb is not unprecedented (see, e.g., full analysis of C II features in SNe Ia in Parrent et al. 2011), SNe with spectra > 1 week before maximum light and strong C II absorption are rare. C II absorption is often an indicator that the SN Ia has other peculiarities, such as in the extremely low-luminosity SN Ia 2008ha (Foley et al. 2009) or the low-velocity SN Ia 2009dc (Taubenberger et al. 2011).

In our first spectroscopic epoch, the C II features are blueshifted to the same velocity of $-11,200 \pm 300 \text{ km s}^{-1}$, which is comparable to the Si II $\lambda 6355$ velocity of $-11,900 \pm 200 \text{ km s}^{-1}$ (i.e., with a C II to Si II velocity ratio of 0.94 ± 0.04). This ratio is low, although nominally consistent with the population of SNe Ia studied in Parrent et al. (2011), and comparable to specific examples such as SNe 1994D and 1996X (Patat et al. 1996; Salvo et al. 2001).

For comparison to our SN 2017ejb spectra in Figure 2, we plot spectra of other peculiar or low-luminosity SNe Ia at similar epochs with respect to *B*-band maximum, including SN 2000cn (Matheson et al. 2008), SN 1986G (Phillips et al. 1987), and SN 2005ke (Matheson et al. 2008). All of the comparison spectra have been de-reddened and the recessional velocity of the SN host galaxy has been removed according to the values in each reference.

⁸ Swope filter functions are provided at <http://csp.obs.carnegiescience.edu/data/filters>

² <https://archive.stsci.edu/>

³ <http://americano.dolphinim.com/dolphot/dolphotACS.pdf>

⁴ <https://acszeropoints.stsci.edu/>

⁵ www.pessto.org

⁶ IRAF, the Image Reduction and Analysis Facility, is distributed by the National Optical Astronomy Observatory, which is operated by the Association of Universities for Research in Astronomy (AURA) under cooperative agreement with the National Science Foundation (NSF).

⁷ from <http://archive.eso.org/cms.html>

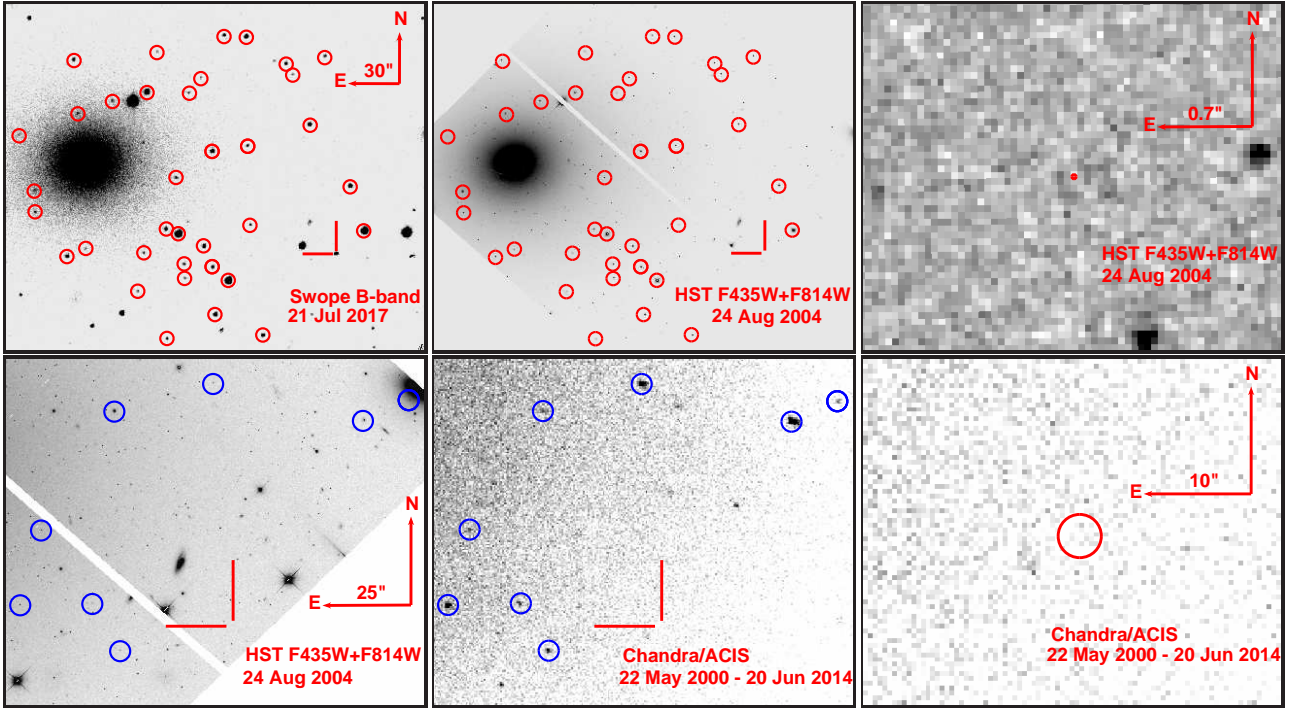


Figure 1. (Top Left) Swope *B*-band image from 21 Jul. 2017 showing SN 2017ejb (red lines) relative to NGC 4696. We circle 36 sources used for relative astrometry with the *HST* image in red. (Top Middle) *HST/ACS F435W+F814W* image of NGC 4696 showing the same region as the image on the left. The location of SN 2017ejb is denoted with red lines. We circle the same 36 sources in the Swope image. (Top Right) A zoom-in of the *HST/F435W+F814W* panel in the middle. We denote the location of SN 2017ejb as determined from relative astrometry with a red circle. The size of the circle corresponds to our astrometric uncertainties ($\approx 0.016''$). There are no sources in the *HST* image within $> 72\sigma$ of the location of SN 2017ejb. (Bottom Left) The same *HST/F435W+F814W* image as above. We circle 8 sources in blue used for relative astrometry. We mark the location of SN 2017ejb with red lines. (Bottom Middle) *Chandra/ACIS* image of the same region on the left. We circle the same 8 sources in the *HST* image in blue and mark the location of SN 2017ejb. (Bottom Right) A zoom-in of the *Chandra/ACIS* image in the middle showing a 4.5 pixel region centered on the location of SN 2017ejb. We do not detect any point-like sources at the $> 3\sigma$ level in this region.

Table 2. Swope Optical Photometry of SN 2017ejb

Epoch	<i>u</i>	<i>B</i>	<i>V</i>	<i>g</i>	<i>r</i>	<i>i</i>
6.82	16.844 (008)	15.785 (006)	15.439 (004)	15.404 (003)	15.447 (003)	15.527 (004)
8.96	16.980 (059)	15.714 (006)	15.300 (004)	15.286 (004)	15.246 (004)	15.407 (004)
12.96	17.455 (040)	15.992 (012)	15.329 (007)	15.402 (007)	15.196 (006)	15.405 (007)
15.00	17.797 (060)	16.219 (016)	15.356 (008)	15.571 (008)	15.252 (005)	15.423 (005)
20.95	18.809 (118)	17.219 (016)	16.014 (008)	16.503 (007)	15.649 (004)	15.673 (006)
31.81	19.524 (148)	18.160 (023)	16.959 (012)	17.433 (012)	16.615 (008)	16.479 (008)
39.93	—	18.476 (040)	17.382 (021)	17.836 (039)	17.272 (022)	17.090 (016)
44.89	—	18.624 (053)	17.594 (027)	17.847 (029)	17.461 (016)	17.245 (013)
54.88	—	18.797 (018)	17.841 (012)	18.192 (013)	17.848 (010)	17.739 (013)
79.81	—	19.320 (057)	18.592 (040)	18.757 (036)	18.914 (058)	18.602 (063)

Note. Epoch is in days relative to discovery on 28.22 May 2017. Uncertainties (1σ) are in millimagnitudes and given in parentheses next to each measurement. All photometry is on the AB scale.

SN 2017ejb shares similarities with all of these objects, especially the velocity and relative ratio of Si II features.

In the VLT/X-shooter spectrum at +2 days after *B*-band maximum, SN 2017ejb exhibits strong, broad Ti II bands characteristic of 1986G-like SNe near $\lambda 4650$ and 5000 (Phillips et al. 1987, also see labels in Figure 2). These lines are much more prominent near peak light than in our pre-maximum spectra. This finding is consistent with the presence of Ti II in SN Ia spectra overall, which is

an indication of relatively low ejecta temperatures (Doull & Baron 2011) where SNe with hotter ejecta have Ti in higher ionization states with fewer and weaker absorption features in the optical.

Finally, although we detect Na I D absorption from the Milky Way with an equivalent width (EW) of $0.7 \pm 0.1 \text{ \AA}$ (which is consistent with the Milky Way reddening of $E(B - V) = 0.098$ mag using the relation in Poznanski et al. 2012), we do not detect any Na I D extinction at the redshift of NGC 4696 at the $< 0.1 \text{ \AA}$ level

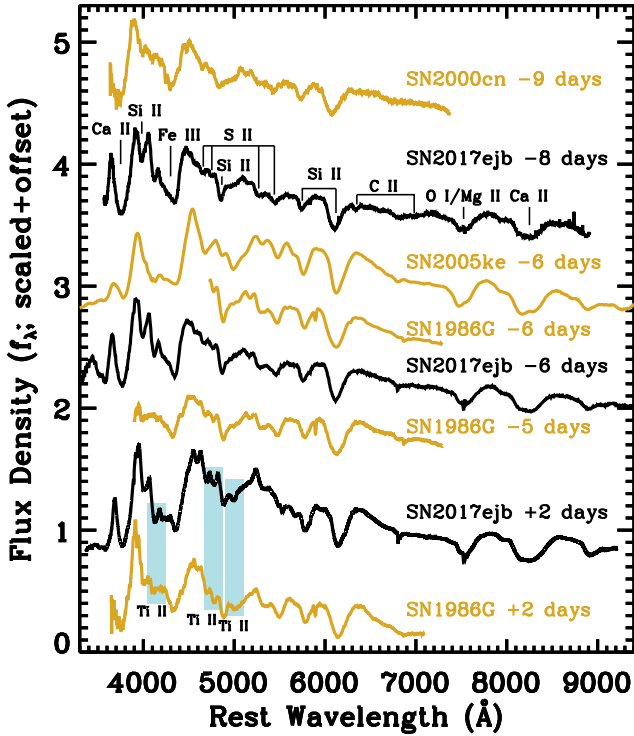


Figure 2. Spectra of SN 2017ejb (black) labeled with the time of observation relative to B -band maximum. In our first epoch, we label several spectroscopic features present. For comparison, we overplot spectra of the low-luminosity SN Ia 2000cn (Matheson et al. 2008), the 1991bg-like SN Ia 2005ke (Folatelli et al. 2013), and the low-luminosity SN Ia 1986G (Phillips et al. 1987). All spectra have been de-reddened for Milky Way and host reddening and their recessional velocities have been removed. We note the presence of Ti II bands (shaded blue) in the SN 2005ke spectrum from 6 days before B maximum, which are either weak or missing in the SN 2017ejb spectra.

in any of our spectra. This implies a host reddening of $E(B-V) < 0.02$ mag. NGC 4696 does have an extended, relatively massive dust lane that was likely captured 10^8 yr ago (de Jong et al. 1990; Sparks et al. 1989). However, SN 2017ejb is $158''$ (28 kpc at the distance of NGC 4696) in projection from the center of its host galaxy. It is unlikely that it would be enshrouded by significant host extinction.

3.2 Light Curves

Assuming the distance and Milky Way extinction above, we plot the extinction-corrected absolute magnitudes for SN 2017ejb in Figure 3. The key characteristics of SN 2017ejb are its low peak magnitude, rapid decline, and apparent lack of a secondary i -band maximum. The B -band light curve peaks around Julian Date 2457910.8 ± 1.0 with $M_B = -17.9 \pm 0.1$ mag and declines with $\Delta m_{B,15} = 1.7 \pm 0.1$ mag. This $\Delta m_{B,15}$ value corresponds to a light curve stretch parameter $x_1 \approx -2.9$ (see, e.g., Guy et al. 2007), which is comparable to many low-luminosity SNe Ia (see distributions in, e.g., Hicken et al. 2009).

Only a small minority of normal SNe Ia have light curve parameters $x_1 < -2.9$ or $\Delta m_{B,15} > 1.7$ mag (e.g., only SNe 1998co and 2007cp out of 146 SNe Ia used for cosmology in Rest et al. 2014). This is partly by design as light curve fitting schemes for cosmology only yield accurate distances for

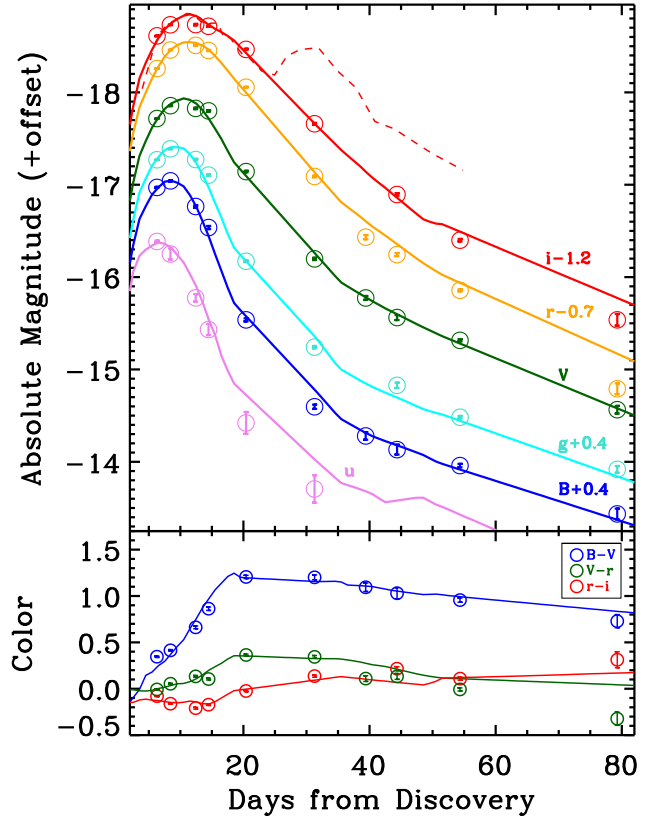


Figure 3. (Top) Swope $uBVgri$ light curves of SN 2017ejb (circles), which have been corrected for Milky Way reddening and shifted to the distance of NGC 4696. For comparison, we overplot Swope in-band SiFTO light curves (solid lines; Conley et al. 2008) based on a SN 1991bg template (Nugent et al. 2002) and fit to the data of SN 2017ejb. We also plot the I -band light curve (dashed red line) of the normal but low-luminosity SN Ia 2007au (Ganeshalingam et al. 2010). All comparison light curves have been corrected for Milky Way extinction and shifted to the distances in their respective references. (Bottom) $B-V$, $V-r$, and $r-i$ color curves of SN 2017ejb (red, green, and blue circles, respectively). We also overplot the SiFTO color curves from the fits in the top panel.

$|x_1| < 3.0$ (e.g., SALT; Guy et al. 2010; Betoule et al. 2014), and SNe outside this range are typically cut from cosmological samples (see, e.g., the homogeneous low-redshift sample in Foley et al. 2018). There are many low-luminosity SNe Ia such as SNe 1986G, 1991bg, 1993H, and 1999by that peak around $M_B = -16.5$ to -18.0 mag and exhibit $\Delta m_{B,15} = 1.7$ – 2.0 mag (Phillips et al. 1987; Filippenko et al. 1992; Garnavich et al. 2004; Altavilla et al. 2004). In this regard, SN 2017ejb appears to fall between the distribution of normal SNe Ia used for cosmology and low-luminosity SNe Ia.

One unusual feature in the SN 2017ejb light curve compared with normal SNe Ia is the apparent lack of a second peak in the i -band light curve, which SNe Ia typically exhibit 20–30 days after peak (even for normal SNe Ia with low values of x_1 ; Kasen 2006). For comparison, we plot the I -band light curve of the low-luminosity but normal SN Ia 2007au (Ganeshalingam et al. 2010), which does exhibit a secondary I -band maximum (dashed red line in Figure 3). SN 2007au has $M_{B,\text{peak}} = -18.0$ mag and very similar light curve parameters to SN 2017ejb (SN 2007au has $x_1 = -2.82$ from Rest et al. 2014). Thus, if SN 2017ejb had been a photometrically normal SN Ia, it is reasonable to expect that

it would have had a prominent secondary *i*-band maximum that would be apparent in our data. SN 2017ejb is more similar to peculiar, low-luminosity SNe Ia in this regard, such as SNe 1986G and 1991bg (Phillips et al. 1987; Filippenko et al. 1992), although with a $\Delta m_{B,15}$ parameter that is on the low end for this population.

In order to find the best-matching light curve template for SN 2017ejb, we performed SiFTO light curve fits (Conley et al. 2008) using a 1991bg-like template from Nugent et al. (2002). We used the Swope filter functions to generate in-band light curves matched to the observed data from SN 2017ejb (Figure 3). The fits are relatively good before and around maximum light, but diverge 50 days into the post-maximum phase (in *r*- and *i*-bands) and in *u*-band generally where most SN Ia light curves are poorly constrained (especially low-luminosity SNe Ia; Taubenberger et al. 2008).

This overall similarity with a peculiar sub-class of SNe Ia, the low peak luminosity, the rapid decline rate compared with most normal SNe Ia, and the lack of a secondary *i*-band maximum seem to indicate that SN 2017ejb is a member of the peculiar, low-luminosity class of SNe Ia such as SNe 1986G and 1991bg. These evidence reinforce the spectroscopic similarity between SN 2017ejb and SN 1986G.

4 PRE-EXPLOSION LIMITS ON A COUNTERPART TO SN 2017EJB

4.1 Relative Astrometry and *HST* Limits

We examined the *Chandra*/ACIS data described above near the explosion site of SN 2017ejb. In order to place constraints on the total number of events associated with the SN 2017ejb progenitor system in the *Chandra* data, we must precisely constrain the location of the explosion site in the *Chandra* images. Archival *Chandra* data products are astrometrically calibrated using the Tycho-2 (Høg et al. 2000), USNO-A2.0 (Urban et al. 1998), and 2MASS (Skrutskie et al. 2006) astrometric catalogs. Similarly, we reduce Swope optical imaging in *photpipe* using 2MASS astrometric standards as described in Kilpatrick et al. (2018). However, we cannot rule out the possibility that there is some systematic offset between *Chandra* and Swope astrometry, and so we cross-checked our astrometric calibration by performing relative astrometry between the *Chandra* and Swope imaging using field sources.

This process is complicated by the fact that bright, compact X-ray sources tend to be extremely faint or extended in optical imaging. Therefore, we aligned our *B*-band image of SN 2017ejb at peak (the 8.96 day epoch in Table 2) to the drizzled *F435W*+*F814W* *HST* image and bootstrapped the relative astrometry to the *Chandra* event map. This process is relatively straightforward given that our Swope *B*-band image covers roughly the same wavelengths as *HST*/ACS *F435W*.

Identifying 36 sources common to our stacked Swope *B*-band image and drizzled *HST* *F435W*+*F814W* image, we performed relative astrometry between the two images. We estimated the uncertainty in our astrometric solution by randomly selecting 18 of these sources and calculating an astrometric solution, then calculating the average offset between the remaining 18 sources. Repeating this process, we estimated the average offset between these sources to be $\sigma_\alpha = 0.014''$ and $\sigma_\delta = 0.013''$. We then determine the location of SN 2017ejb using coordinates from *photpipe*. SN 2017ejb is detected at $\sim 160\sigma$ in the Swope *B*-band image with a full-width at half-maximum of $1.3''$, and so we estimate that the

approximate location of the SN contributes $\approx 0.008''$ to the astrometric uncertainty. At the location of SN 2017ejb, we do not detect any sources at the $\geq 3\sigma$ level in the individual or stacked *HST* images. The closest source of any kind is detected at 8.9σ in the drizzled *F435W*+*F814W* image and is $1.15''$ away from the location of SN 2017ejb, or about 72 times the total astrometric uncertainty (Figure 1). Thus, we conclude that there is no source in any of these images consistent with being the progenitor system of SN 2017ejb.

We then identified 8 sources common to the drizzled *HST* image and *Chandra* image (Figure 1). Using *sextractor* to determine the centroids of these sources in the *Chandra* image, we repeated the same process above, with 4 sources to calculate a WCS solution and using the remaining 4 sources to estimate the average offset. We found an average offset of $\sigma_\alpha = 0.10''$ and $\sigma_\delta = 0.08''$. Therefore, the combined uncertainty in the position of SN 2017ejb in the *Chandra* image using our Swope→*HST*→*Chandra* relative astrometry is approximately $0.11''$, or roughly 0.22 *Chandra* pixels.

We also used *dolphot* to estimate the 3σ limiting magnitude on the presence of a source in the *F435W* and *F814W* images. Using the *FakeStar* parameter, we injected 10000 sources with a fixed number of counts into the *flc* files. We chose the positions for each of these sources by generating Gaussian random variables x, y centered at the best-fitting pixel coordinates of SN 2017ejb and with standard deviations corresponding to the astrometric uncertainty in our relative astrometry on the location of SN 2017ejb (0.32 ACS/WFC pixels). We increased the number of counts associated with these sources and repeated the process until we recovered ≥ 9970 sources at the $\geq 3\sigma$ level. In this way, we determined that the 3σ limiting magnitude on the presence of a point source at the location of SN 2017ejb to be $m_{F435W} > 28.3$ mag and $m_{F814W} > 26.8$ mag.

For the distance and Milky Way extinction to NGC 4696, the *HST* limits correspond to $M_{F435W} > -5.2$ mag and $M_{F814W} > -6.4$ mag. Even for a relatively small bolometric correction (e.g., $BC_{F435W} = 0$), the *F435W* limiting magnitude corresponds to a source with $\log(L/L_\odot) = 4.0$, which is approximately the luminosity of a $13 M_\odot$ main-sequence star based on Mesa Isochrone & Stellar Track evolutionary models (Paxton et al. 2011, 2013, 2015; Dotter 2016; Choi et al. 2016)⁹. For stars with redder colors (i.e., where the *F814W* bolometric correction is small), we can rule out stars with $\log(L/L_\odot) = 4.5$, which corresponds $M_{init} = 10$ – $13 M_\odot$ red supergiants. These limits are not very constraining in the context of SN Ia progenitor systems — high-mass stars in this range would explode before a WD could evolve.

4.2 *Chandra* Limits

Although there are events detected near the location of SN 2017ejb in the *Chandra* image, this emission is smooth and likely associated with the hot gas surrounding NGC 4696 (as analyzed in, e.g., Crawford et al. 2005; Fabian et al. 2005). Following methods described in Nielsen et al. (2012), we considered the total number of counts within a 4.5 pixel radius of the location of SN 2017ejb as this is where $>95\%$ of the energy is encircled for a point source observed by *Chandra*/ACIS¹⁰. Within a 4.5 pixel radius of the location of SN 2017ejb, we detected a total of 509 counts in the 0.3–

⁹ <http://waps.cfa.harvard.edu/MIST/>

¹⁰ see <http://cxc.harvard.edu/proposer/POG/html/>

1.0 keV *Chandra*/ACIS soft bandpass (Figure 1). There is no evidence for a point-like source at this location.

As in Gehrels (1986) and Nielsen et al. (2012), we calculated the maximum average number of counts μ for which the probability of observing $x \leq N$ counts (where, here, $N = 509$) is within 3σ (i.e., $P(\mu; x \leq N) \leq 0.0013$). Since the observed number of counts N is large, we approximated the value of μ using equation (9) in Gehrels (1986) for a 3σ limit to be $\mu \approx 581$. This value represents the maximum 3σ limit on a 0.3–1.0 keV source at the location of SN 2017ejb, which includes background counts.

In order to remove the contribution from background counts, we calculated the number of counts per pixel around the location of SN 2017ejb using an annulus with inner radius 9 pixels and outer radius 18 pixels. The average number of counts per pixel is $8.02 \text{ ct pixel}^{-1}$, and so we approximated the maximum number of counts for a 3σ detection of a source at the location of SN 2017ejb to be $\mu' \approx 581 - \pi \times (4.5)^2 \times 8.02 = 70.8$. This value is roughly consistent with the 3σ limit derived by assuming that the source is entirely dominated by Poisson noise from the background (i.e., $3 \times \sqrt{\pi \times (4.5)^2 \times 8.02} = 67.8$). Therefore, we are confident that 70.8 ct is a conservative 3σ limit on the total 0.3–1.0 keV counts from any pre-explosion counterpart to SN 2017ejb.

The flux limit in the 0.3–1.0 keV band depends on the effective exposure map at the location of SN 2017ejb for the merged *Chandra*/ACIS data. We generated a weighted exposure map by assuming that any source detected at the location of SN 2017ejb would have a 0.3–1.0 keV spectral profile resembling an absorbed blackbody. Using CIAO/xabsphot, we modeled absorbed blackbodies with temperatures in the range $kT = 20\text{--}200 \text{ eV}$ (corresponding to the full range of observed SSS temperatures in, e.g., van den Heuvel et al. 1992; Kahabka & Ergma 1997; Ness et al. 2013).

For the total column of hydrogen to NGC 4696, we note that the Milky Way extinction quoted above corresponds to $N_H = 6.76 \times 10^{20} \text{ cm}^{-2}$ using the best-fitting scaling relation in Güver & Özel (2009). There is effectively zero host extinction to SN 2017ejb based on the absence of any Na I D absorption in its optical spectrum, and so we do not account for any column of hydrogen in the host galaxy. However, we cannot rule out the possibility that there is circumstellar extinction originating from gas or dust around the progenitor system of SN 2017ejb and close enough that it would have been destroyed within the first few days after explosion (i.e., before we obtained our spectrum such that the Na I D is variable, as in Patat et al. 2007; Simon et al. 2009). We do not account for any such circumstellar extinction, but we acknowledge that this is a possibility for a WD accreting from a companion wind or in a symbiotic binary (although it has been found that circumstellar extinction has little effect on the inferred X-ray luminosities for SSS temperatures $> 30 \text{ eV}$ and accretion rates $< 10^{-6} M_\odot \text{ yr}^{-1}$; Nielsen & Gilfanov 2015).

For every model spectrum, we calculated the value of the *Chandra*/ACIS exposure map at the location of SN 2017ejb (ζ in $\text{cm}^2 \text{ s}$) and the average energy per photon in the 0.3–1.0 keV band ($\langle E \rangle$). Thus, the 3σ upper limit on the 0.3–1.0 keV X-ray luminosity from the combined *Chandra* data is

$$L_X = \frac{4\pi\mu'\langle E \rangle d^2}{\zeta} \quad (1)$$

for the values of the 3σ count limit μ' and distance d given above. In order to convert this upper limit to a bolometric luminosity, we

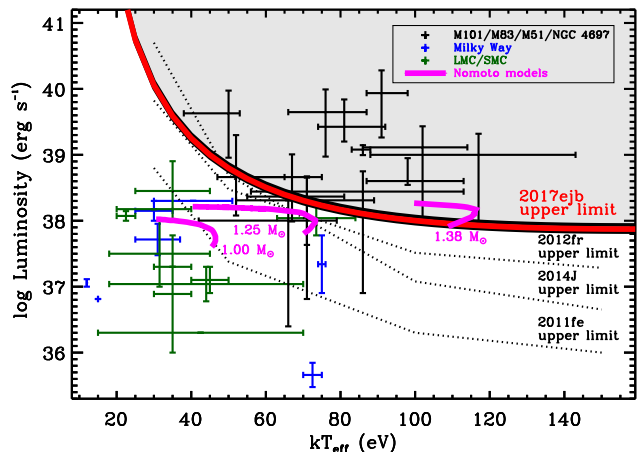


Figure 4. Hertzsprung-Russell diagram of supersoft X-ray sources (SSS). We overplot the temperatures and luminosities of known SSS systems in M51, M81, M83, M101, NGC 4697 (black; from Swartz et al. 2002; Di Stefano & Kong 2003), the LMC, SMC, and Milky Way (green and blue; from Greiner 2000). For comparison, we overplot a model of a $1.38 M_\odot$ stably-accreting WDs (magenta lines) with masses 1.00, 1.25, and $1.38 M_\odot$ from Nomoto et al. (2007). The derived limits on SSS systems of varying temperatures are shown for SNe 2011fe, 2012fr (Nielsen et al. 2013), 2014J (Nielsen et al. 2014), and 2017ejb (this paper). We can rule out the hottest and most luminous SSS systems (grey region) as the progenitor of SN 2017ejb as well as the Chandrasekhar-mass WD accreting at rates $> 3 \times 10^{-8} M_\odot$.

calculated the fraction of the unabsorbed blackbody spectrum with temperature T_{eff} in the 0.3–1.0 keV band as

$$c(T_{\text{eff}}) = \frac{\int_{0.3 \text{ keV}}^{1.0 \text{ keV}} B_E(T_{\text{eff}}) dE}{\int_0^\infty B_E(T_{\text{eff}}) dE} \quad (2)$$

where $B_E(T)$ is the energy-dependent Planck function for a temperature T . Thus, the upper limit on the bolometric luminosity for a model spectrum with effective temperature T_{eff} is $L_{\text{bol}} = L_X / c(T_{\text{eff}})$. We show our upper limit (red) on the bolometric luminosity of any SSS counterpart to SN 2017ejb as a function of the assumed model temperature kT_{eff} in Figure 4. We also show the effect of varying the distance to the Centaurus cluster within the 1σ uncertainties (black), which only has a marginal effect on the limiting luminosity.

5 DISCUSSION

Our upper limit on the bolometric luminosity of any SSS is comparable to similar limits presented in Nielsen et al. (2012) and Nielsen et al. (2014) as shown in Figure 4. In particular, the limits on a SSS counterpart at low temperatures are comparable to those for SNe 2014J and 2012fr, though not as constraining as for SN 2011fe. For comparison, we show several known SSS systems (from Greiner 2000; Swartz et al. 2002; Di Stefano & Kong 2003) as well as models for a Chandrasekhar-mass ($1.38 M_\odot$) and sub-Chandrasekhar mass (1.00 and $1.25 M_\odot$) stably-accreting SSS with accretion rates 10^{-8} to $2.5 \times 10^{-7} M_\odot \text{ yr}^{-1}$ from Nomoto et al. (2007).

Our 3σ limits for SN 2017ejb are $L_{\text{bol}} = 1.78 \times 10^{39} \text{ erg s}^{-1}$ at 40 eV, $L_{\text{bol}} = 3.20 \times 10^{39} \text{ erg s}^{-1}$ at 60 eV, and $L_{\text{bol}} = 1.00 \times 10^{38} \text{ erg s}^{-1}$ at 100 eV. These limits rule out all known

sources hotter than $kT_{\text{eff}} = 85$ eV and more luminous than $L_{\text{bol}} = 4 \times 10^{38}$ erg s⁻¹. The comparison SSS systems include a number of sources in M51, M81, M83, and M101 identified by [Swartz et al. \(2002\)](#) and [Di Stefano & Kong \(2003\)](#) using *Chandra*, and so are systematically hotter and more luminous than sources identified, for example, in the Milky Way, LMC, and SMC using *ROSAT* ([Greiner 2000](#)). We also rule out stably-accreting Chandrasekhar-mass WDs (in particular, those in the temperature range expected for SSS systems; [Nomoto et al. 2007](#)) with the highest mass-loss rates ($> 3 \times 10^{-8} M_{\odot} \text{ yr}^{-1}$).

However, we cannot definitively rule out certain types of accreting WDs that lead to anomalously cool or low-luminosity SSS systems, for example, due to WD spin down (e.g., [Di Stefano et al. 2011](#)). In this scenario, an accreting WD can reach the Chandrasekhar mass but must spin-down and cool before it can explode. In general, these scenarios are disfavored, as they would imply that most galaxies host a large population of rapidly-spinning WDs that will soon explode as SNe Ia, which is not observed (e.g., [Norton et al. 2004](#); [Ferrario & Wickramasinghe 2005](#)).

Another important caveat is that our most recent epoch of pre-explosion X-ray data was obtained roughly 3 years before SN 2017ejb was discovered. We are completely insensitive to any pre-explosion X-ray emission within those 3 years. Furthermore, the bulk of the X-ray data (486.25 ks) were obtained around 3 year before discovery, but we are significantly less sensitive to X-ray sources in this period than over the full 14 years of observations. If the SN Ia ignition mechanism involves rapid mass transfer onto a WD on timescales comparable to or less than ~ 3 years before explosion, we would not have detected any signature from that event.

We are also insensitive to circumstellar material in the immediate environment of the progenitor system that would be promptly destroyed and undetectable in the early-time spectra. In general, such a large mass of material is not unexpected as optical and radio observations rule out large column densities of hydrogen in the immediate environments of SN Ia progenitor systems ([Leonard 2007](#); [Shappee et al. 2013](#); [Chomiuk et al. 2012, 2016](#)). Moreover, if a companion star to the WD progenitor of SN 2017ejb was losing mass at rates of $> 10^{-6} M_{\odot} \text{ yr}^{-1}$ (i.e., where circumstellar extinction would have a significant effect on a SSS spectral profile; [Nielsen & Gilfanov 2015](#)), then the WD would likely be accreting at a high rate and produce a luminous X-ray source. We rule out stably accreting WDs with mass accretion rates around $3 \times 10^{-8} - 2.5 \times 10^{-7} M_{\odot} \text{ yr}^{-1}$, and so it is unlikely SN 2017ejb exploded from a system with an even higher accretion rates (and intrinsic luminosities) > 4 times as large but some circumstellar extinction.

Overall, there is significant parameter space within which an accreting WD progenitor system to SN 2017ejb could have undergone a Chandrasekhar or sub-Chandrasekhar mass explosion. If the progenitor WD had a sub-Chandrasekhar mass ($< 1.35 M_{\odot}$), or had a low accretion rate ($< 3 \times 10^{-8} M_{\odot} \text{ yr}^{-1}$), or underwent rapid mass-transfer within the last few years before explosion, we would not have detected an X-ray source. Any of these scenarios is plausible, but together they add context to the characteristics and large-scale environment of the SN 2017ejb explosion.

In particular, we note that SN 2017ejb was discovered in the massive elliptical galaxy NGC 4696 ([Shobbrook 1963](#); [Mitchell et al. 1975](#)). While this galaxy exhibits tendrils of dust that likely originate from material captured 10^8 yr ago, most of the star formation in NGC 4696 is suppressed by its central black hole ([Sanders et al. 2016](#)). SN 2017ejb is also at least 20 kpc in projection from these dust lanes, implying that if the progenitor system originated from a burst of star formation in this material, it

must have had a projected velocity ≥ 200 km s⁻¹ very soon after it formed. This scenario is plausible if the stars produced in this burst maintained some of the velocity from the infalling material. On the other hand, the progenitor system could also have originated from a previous burst of star formation in NGC 4696 and before its central black hole became highly active. This scenario would support the conclusions of studies such as [Howell \(2001\)](#) and [Piro et al. \(2014\)](#), who point to older stellar populations in galaxies with low star formation as likely sites for binary WD mergers. In addition, our findings support the hypothesis that some low-luminosity SNe Ia may be the result of binary WD mergers ([Pakmor et al. 2010](#)).

Combined with the growing sample of optical and X-ray limits in the literature ([Nelemans et al. 2008](#); [Maiz & Mannucci 2008](#); [Li et al. 2011](#); [Nielsen et al. 2013, 2014](#); [Kelly et al. 2014](#)), the SN 2017ejb limits rule out interesting regions in WD temperature and luminosity for plausible progenitor systems. In particular, we can rule out most systems near the Chandrasekhar limit, assuming they were stably accreting for years before explosion. Combined with the limits from SNe 2011fe, 2012fr, and 2014J, we conclude at the 95% confidence level that $< 47\%$ of SNe Ia explode from systems involving a stably-accreting Chandrasekhar-mass SSS.

Future analysis of pre-explosion imaging for all SNe Ia can be used to verify or constrain expectations for the configuration of their progenitor systems and explosion scenarios. In light of the wide variety of SN Ia explosion models, this type of analysis provides one of the most promising lines of inquiry for resolving the SN Ia progenitor problem.

6 CONCLUSIONS

We analyze post-explosion imaging and spectroscopy of SN 2017ejb and pre-explosion *HST* and *Chandra* imaging of its explosion site. In summary, we find:

(i) SN 2017ejb is a low-luminosity SN Ia with strong C II absorption features in its pre-maximum spectra. Photometrically, it has a low peak luminosity, it declines quickly, and it lacks a secondary *i*-band maximum. Spectroscopically, it is similar to SN 1986G, but with relatively weak Ti II bands. Overall, it is most similar to low-luminosity SNe Ia such as SNe 1986G and 1991bg.

(ii) We do not detect any counterpart to SN 2017ejb in pre-explosion *Chandra* imaging. Assuming that any pre-explosion *Chandra* source resembles a blackbody obscured by Milky Way extinction, our limits correspond to $L_{\text{bol}} = 4 \times 10^{38}$ erg s⁻¹ at most feasible effective temperatures. These limits rule out a SSS system similar to any in the literature with $kT_{\text{eff}} > 85$ eV as well as models of accreting, Chandrasekhar-mass WDs with accretion rates $\dot{M} > 3 \times 10^{-8} M_{\odot} \text{ yr}^{-1}$.

(iii) These limits are consistent with WD progenitors that are either low-mass, have low accretion rates, or undergo mass transfer very soon before explosion. Combined with the limits from other nearby systems, we infer that $< 47\%$ of SNe Ia explode from systems involving a stably-accreting Chandrasekhar-mass SSS.

ACKNOWLEDGMENTS

We thank J. Anais, A. Campillay, and S. Castellón for assistance with Swope observations.

The UCSC team is supported in part by NASA grant NNG17PX03C, NSF grant AST-1518052, the Gordon & Betty Moore Foundation, the Heising-Simons Foundation, and by fellowships from the Alfred P. Sloan Foundation and the David and Lucile Packard Foundation to R.J.F.

This work includes data obtained with the Swope Telescope at Las Campanas Observatory, Chile, as part of the Swope Time Domain Key Project (PI Piro, Co-PIs Drout, Foley, Hsiao, Madore, Phillips, and Shappee). This work is based in part on observations collected at the European Organisation for Astronomical Research in the Southern Hemisphere, Chile as part of PESSTO (the Public ESO Spectroscopic Survey for Transient Objects Survey) ESO programmes 188.D-3003, 191.D-0935, and 197.D-1075. This work is based in part on observations made with ESO Telescopes at the La Silla Paranal Observatory under programme ID 099.D-0641 (PI Maguire).

The *Hubble Space Telescope* (*HST*) is operated by NASA/ESA. Some of our analysis is based on data obtained through programme GO-9427 (PI Harris) from the *HST* archive operated by STScI.

The scientific results reported in this article are based in part on observations made by the *Chandra* X-ray Observatory and published previously in cited articles. We obtained these data from the *Chandra* Data Archive.

Facilities: *HST* (ACS), *Chandra* (ACIS), VLT (X-shooter), SOAR (Goodman), NTT (EFOSC), Swope (Direct)

REFERENCES

- Altavilla G., et al., 2004, *MNRAS*, **349**, 1344
- Ashall C., Mazzali P., Sasdelli M., Prentice S. J., 2016, *MNRAS*, **460**, 3529
- Betoule M., et al., 2014, *A&A*, **568**, A22
- Cartier R., et al., 2017, *MNRAS*, **464**, 4476
- Choi J., Dotter A., Conroy C., Cantiello M., Paxton B., Johnson B. D., 2016, *ApJ*, **823**, 102
- Chomiuk L., et al., 2012, *ApJ*, **750**, 164
- Chomiuk L., et al., 2016, *ApJ*, **821**, 119
- Clemens J. C., Crain J. A., Anderson R., 2004, in Moorwood A. F. M., Iyem M., eds, Proc. SPIE Vol. 5492, Ground-based Instrumentation for Astronomy. pp 331–340, doi:10.1117/12.550069
- Conley A., et al., 2008, *ApJ*, **681**, 482
- Cooper M. C., Newman J. A., Yan R., 2009, *ApJ*, **704**, 687
- Crawford C. S., Hatch N. A., Fabian A. C., Sanders J. S., 2005, *MNRAS*, **363**, 216
- Dan M., Rosswog S., Guillochon J., Ramirez-Ruiz E., 2012, *MNRAS*, **422**, 2417
- Di Stefano R., 2010, *ApJ*, **712**, 728
- Di Stefano R., Kong A. K. H., 2003, *ApJ*, **592**, 884
- Di Stefano R., et al., 2004, *ApJ*, **610**, 247
- Di Stefano R., Voss R., Claeys J. S. W., 2011, *ApJ*, **738**, L1
- Dolphin A. E., 2000, *PASP*, **112**, 1383
- Dotter A., 2016, *ApJS*, **222**, 8
- Doull B. A., Baron E., 2011, *PASP*, **123**, 765
- Edlund J. A., Tinto M., Królak A., Nelemans G., 2005, *Classical and Quantum Gravity*, **22**, S913
- Fabian A. C., Sanders J. S., Taylor G. B., Allen S. W., 2005, *MNRAS*, **360**, L20
- Ferrario L., Wickramasinghe D. T., 2005, *MNRAS*, **356**, 615
- Filippenko A. V., 1997, *ARA&A*, **35**, 309
- Filippenko A. V., et al., 1992, *AJ*, **104**, 1543
- Fink M., Hillebrandt W., Röpke F. K., 2007, *A&A*, **476**, 1133
- Fink M., Röpke F. K., Hillebrandt W., Seitenzahl I. R., Sim S. A., Kromer M., 2010, *A&A*, **514**, A53
- Finzi A., Wolf R. A., 1967, *ApJ*, **150**, 115
- Folatelli G., et al., 2013, *ApJ*, **773**, 53
- Foley R. J., Kasen D., 2011, *ApJ*, **729**, 55
- Foley R. J., et al., 2009, *AJ*, **138**, 376
- Foley R. J., et al., 2012, *ApJ*, **752**, 101
- Foley R. J., et al., 2016, *MNRAS*, **461**, 1308
- Foley R. J., et al., 2018, *MNRAS*, **475**, 193
- Fruscione A., Siemiginowska A., 1999, NASA STI/Recon Technical Report N. 99
- Ganeshalingam M., et al., 2010, *ApJS*, **190**, 418
- Garnavich P. M., et al., 2004, *ApJ*, **613**, 1120
- Gehrels N., 1986, *ApJ*, **303**, 336
- Greiner J., 2000, *New Astron.*, **5**, 137
- Guillochon J., Dan M., Ramirez-Ruiz E., Rosswog S., 2010, *ApJ*, **709**, L64
- Güver T., Özel F., 2009, *MNRAS*, **400**, 2050
- Guy J., et al., 2007, *A&A*, **466**, 11
- Guy J., et al., 2010, *A&A*, **523**, A7
- Hansen C. J., Wheeler J. C., 1969, *Ap&SS*, **3**, 464
- Hicken M., et al., 2009, *ApJ*, **700**, 331
- Høg E., et al., 2000, *A&A*, **355**, L27
- Howell D. A., 2001, *ApJ*, **554**, L193
- Hoyle F., Fowler W. A., 1960, *ApJ*, **132**, 565
- Iben Jr. I., Tutukov A. V., 1984, *ApJS*, **54**, 335
- Jester S., et al., 2005, *AJ*, **130**, 873
- Jones D. O., et al., 2013, *ApJ*, **768**, 166
- Kahabka P., Ergma E., 1997, *A&A*, **318**, 108
- Kasen D., 2006, *ApJ*, **649**, 939
- Kelly P. L., et al., 2014, *ApJ*, **790**, 3
- Kilpatrick C. D., et al., 2018, *MNRAS*, **473**, 4805
- Kushnir D., Katz B., Dong S., Livne E., Fernández R., 2013, *ApJ*, **778**, L37
- Lentz E. J., Baron E., Branch D., Hauschildt P. H., Nugent P. E., 2000, *ApJ*, **530**, 966
- Leonard D. C., 2007, *ApJ*, **670**, 1275
- Li W., et al., 2011, *Nature*, **480**, 348
- Maeda K., Katsuna M., Shigeyama T., 2014, *ApJ*, **794**, 37
- Mandel K. S., Foley R. J., Kirshner R. P., 2014, *ApJ*, **797**, 75
- Maoz D., Mannucci F., 2008, *MNRAS*, **388**, 421
- Maoz D., Mannucci F., Nelemans G., 2014, *ARA&A*, **52**, 107
- Matheson T., et al., 2008, *AJ*, **135**, 1598
- Mazzali P. A., et al., 2015, *MNRAS*, **450**, 2631
- McCully C., et al., 2014, *Nature*, **512**, 54
- Mieske S., Hilker M., 2003, *A&A*, **410**, 445
- Mitchell R. J., Charles P. A., Culhane J. L., Davison P. J. N., Fabian A. C., 1975, *ApJ*, **200**, L5
- Modigliani A., et al., 2010, in Observatory Operations: Strategies, Processes, and Systems III. p. 773728, doi:10.1117/12.857211
- Nelemans G., Voss R., Roelofs G., Bassa C., 2008, *MNRAS*, **388**, 487
- Ness J.-U., et al., 2013, *A&A*, **559**, A50
- Nielsen M. T. B., Gilfanov M., 2015, *MNRAS*, **453**, 2927
- Nielsen M. T. B., Nelemans G., Voss R., 2011, preprint, (arXiv:1101.5949)
- Nielsen M. T. B., Voss R., Nelemans G., 2012, *MNRAS*, **426**, 2668
- Nielsen M. T. B., Voss R., Nelemans G., 2013, *MNRAS*, **435**, 187
- Nielsen M. T. B., Gilfanov M., Bogdán Á., Woods T. E., Nelemans G., 2014, *MNRAS*, **442**, 3400
- Nomoto K., 1982, *ApJ*, **253**, 798
- Nomoto K., Saio H., Kato M., Hachisu I., 2007, *ApJ*, **663**, 1269
- Norton A. J., Wynn G. A., Somerscales R. V., 2004, *ApJ*, **614**, 349
- Nugent P., Kim A., Perlmutter S., 2002, *PASP*, **114**, 803
- Pakmor R., Kromer M., Röpke F. K., Sim S. A., Ruiter A. J., Hillebrandt W., 2010, *Nature*, **463**, 61
- Pakmor R., Kromer M., Taubenberger S., Sim S. A., Röpke F. K., Hillebrandt W., 2012, *ApJ*, **747**, L10
- Pan Y.-C., et al., 2014, *MNRAS*, **438**, 1391
- Pan Y.-C., Reed D. K., Medallion M. S., Foley R. J., Jha S. W., Rest A., Scolnic D., 2017, The Astronomer's Telegram, **10437**
- Parrent J. T., et al., 2011, *ApJ*, **732**, 30
- Patat F., Benetti S., Cappellaro E., Danziger I. J., della Valle M., Mazzali P. A., Turatto M., 1996, *MNRAS*, **278**, 111
- Patat F., et al., 2007, *Science*, **317**, 924
- Paxton B., Bildsten L., Dotter A., Herwig F., Lesaffre P., Timmes F., 2011, *ApJS*, **192**, 3
- Paxton B., et al., 2013, *ApJS*, **208**, 4
- Paxton B., et al., 2015, *ApJS*, **220**, 15
- Perlmutter S., et al., 1999, *ApJ*, **517**, 565
- Phillips M. M., et al., 1987, *PASP*, **99**, 592
- Phillips M. M., Lira P., Suntzeff N. B., Schommer R. A., Hamuy M., Maza J., 1999, *AJ*, **118**, 1766
- Piro A. L., Thompson T. A., Kochanek C. S., 2014, *MNRAS*, **438**, 3456
- Poznanski D., Prochaska J. X., Bloom J. S., 2012, *MNRAS*, **426**, 1465

- Raskin C., Scannapieco E., Rockefeller G., Fryer C., Diehl S., Timmes F. X., 2010, *ApJ*, **724**, 111
- Rest A., et al., 2005, *ApJ*, **634**, 1103
- Rest A., et al., 2014, *ApJ*, **795**, 44
- Riess A. G., et al., 1998, *AJ*, **116**, 1009
- Riess A. G., et al., 2016, *ApJ*, **826**, 56
- Rosswog S., Kasen D., Guillochon J., Ramirez-Ruiz E., 2009, *ApJ*, **705**, L128
- Rubin D., et al., 2017, preprint, ([arXiv:1707.04606](https://arxiv.org/abs/1707.04606))
- Salvo M. E., Cappellaro E., Mazzali P. A., Benetti S., Danziger I. J., Patat F., Turatto M., 2001, *MNRAS*, **321**, 254
- Sanders J. S., et al., 2016, *MNRAS*, **457**, 82
- Schlafly E. F., Finkbeiner D. P., 2011, *ApJ*, **737**, 103
- Scolnic D. M., et al., 2017, preprint, ([arXiv:1710.00845](https://arxiv.org/abs/1710.00845))
- Shappee B. J., Stanek K. Z., Pogge R. W., Garnavich P. M., 2013, *ApJ*, **762**, L5
- Shen K. J., Bildsten L., 2009, *ApJ*, **699**, 1365
- Shen K. J., Bildsten L., 2014, *ApJ*, **785**, 61
- Shobbrook R. R., 1963, *The Observatory*, **83**, 36
- Simon J. D., et al., 2009, *ApJ*, **702**, 1157
- Skrutskie M. F., et al., 2006, *AJ*, **131**, 1163
- Smartt S. J., et al., 2015, *A&A*, **579**, A40
- Sparks W. B., Macchetto F., Golombek D., 1989, *ApJ*, **345**, 153
- Sullivan M., et al., 2010, *MNRAS*, **406**, 782
- Swartz D. A., Ghosh K. K., Suleimanov V., Tennant A. F., Wu K., 2002, *ApJ*, **574**, 382
- Taam R. E., 1980, *ApJ*, **242**, 749
- Tartaglia L., Sand D., Wyatt S., Valenti S., Bostroem K. A., Reichart D. E., Haislip J. B., Kouprianov V., 2017, *The Astronomer's Telegram*, **10439**
- Taubenberger S., et al., 2008, *MNRAS*, **385**, 75
- Taubenberger S., et al., 2011, *MNRAS*, **412**, 2735
- Thompson T. A., 2011, *ApJ*, **741**, 82
- Urban S. E., Corbin T. E., Wycoff G. L., 1998, *AJ*, **115**, 2161
- Valenti S., Hosseinzadeh G., Arcavi I., McCully C., Howell D. A., Sand D., Tartaglia L., 2017, *The Astronomer's Telegram*, **10438**
- Webbink R. F., 1984, *ApJ*, **277**, 355
- Whelan J., Iben Jr. I., 1973, *ApJ*, **186**, 1007
- Wolf C., et al., 2018, *Publ. Astron. Soc. Australia*, **35**, e010
- de Jong T., Norgaard-Nielsen H. U., Jorgensen H. E., Hansen L., 1990, *A&A*, **232**, 317
- van den Heuvel E. P. J., Bhattacharya D., Nomoto K., Rappaport S. A., 1992, *A&A*, **262**, 97